

Analytical Methods

Accepted Manuscript



This is an *Accepted Manuscript*, which has been through the Royal Society of Chemistry peer review process and has been accepted for publication.

Accepted Manuscripts are published online shortly after acceptance, before technical editing, formatting and proof reading. Using this free service, authors can make their results available to the community, in citable form, before we publish the edited article. We will replace this *Accepted Manuscript* with the edited and formatted *Advance Article* as soon as it is available.

You can find more information about *Accepted Manuscripts* in the [Information for Authors](#).

Please note that technical editing may introduce minor changes to the text and/or graphics, which may alter content. The journal's standard [Terms & Conditions](#) and the [Ethical guidelines](#) still apply. In no event shall the Royal Society of Chemistry be held responsible for any errors or omissions in this *Accepted Manuscript* or any consequences arising from the use of any information it contains.



Analytical Methods

ARTICLE

Characterization of colorimetric sensor array by multi-spectral technique[†]

Li Zhihua^a, Zhou Xucheng^a, Zou Xiaobo^{a,*}, Shi Jiyong^a, Huang Xiaowei^a, Haroon Elrasheid Tahir^a, Shen Tingting^a

Received 00th January 20xx,
Accepted 00th January 20xx

DOI: 10.1039/x0xx00000x

www.rsc.org/

A new method based on multi-spectral technique was proposed to characterize the signal of colorimetric sensor array for gas detection. Firstly, the characteristic wavelengths, which are most relevant to the detected substance, were extracted from the hyperspectral information of the colorimetric sensor arrays. Then, narrowband filters with the corresponding central wavelengths were selected to isolate the effective signal of the sensor arrays. In this study, ammonia (NH₃) was taken as example to test the performance of the proposed multi-spectral method. Prediction of NH₃ concentration based on the hyperspectral method and normal tri-color (R/G/B) method was also performed for comparison. Compared with the tri-color method, the correlation coefficient for testing set (R_t) based on the multi-spectral method increased from 0.902 to 0.976, root mean squared error of prediction (RMSEP) decreased from 1.213 to 0.548, and residual predictive deviation for testing set (RPD_t) increased from 2.903 to 6.151, which means that the results were improved obviously both in accuracy and stability. Furthermore, the multi-spectral method still possesses the advantages, as low-cost, easy operating and greatly reduced data size. The proposed multi-spectral method could be used to characterize the signal of the colorimetric sensor arrays for gas detection.

1. Introduction

The colorimetric sensor array, which mimics mammalian olfactory or gustatory system, is a novel sensing technique developed in recent years¹⁻⁴. The chemically responsive dyes used to fabricate colorimetric sensor arrays usually have open coordination sites for intense coloration and axial ligation. Interactions such as π - π molecular complexation, bond formation, acid-base interaction, physical adsorption, van der Waals interaction could take place when they were exposed to different analytes⁵. These interactions change the optical property of a colorimetric sensor array which presents different colors or spectra⁶. Combined with certain chemometric methods, qualitative or quantitative analysis could be realized utilizing the response signal of all dyes in the array. At present, the colorimetric sensor arrays have been widely applied in the detection of various substances, e.g., metal ions^{7,8}, toxic industrial chemicals^{6,9,10}, volatile organic compounds¹¹⁻¹⁴, amines³, formaldehyde¹⁵, explosives¹⁶, hydrogen sulfide¹⁷, etc.

Generally, the response signal of the sensor arrays could be characterized through two methods, i.e., spectroscopic method and tri-color imaging method as reported by many authors^{2, 12, 18, 19}. The spectroscopic method is highly advantageous because its integrated spectra contain massive

information. However, it always needs complex equipment and certain time to obtain the spectrum from each sensor element, and it is not suitable for sensors with a solid opaque substrate and gas detection. Furthermore, only part of the dye spot could be covered since the focal region of the spectroscopic detector is relative limit, which means unavoidable operation error. Compared with spectroscopic method, the tri-color imaging methods could detect several sensing elements in a given field of view and are easier to operate and need no special instruments²⁰, which could be a common digital camera, flatbed scanner, cellphone camera, etc. However, the tri-color imaging method usually provide only three or four channels, i.e., red, green and blue (RGB), sometimes red, yellow, green and blue (RYGB). Thus, the information collected by the tri-color imaging methods is significantly less than that of spectroscopic method. However, the detected three channels are highly correlated to each other and contained relatively high noise because the response wavelength range of the three kinds of photosensitive units of a camera is wide and overlapping.

It is necessary to explore a new method to collect the most useful information of the colorimetric sensor array, while keeping the advantages as low-cost and easy operating. To perform this task, the characteristic wavelengths, which are most relevant to the detected substance, must be extracted from the full wavelength range first, then the signal change of the colorimetric sensor arrays at the characteristic wavelengths should be acquired with a simple device. With this consideration, a multi-spectral method was developed to characterize the signal of the colorimetric sensor arrays based on our former studies²¹⁻²⁵. Firstly, hyperspectral imaging technique, which could provide both spatial and spectral

^a College of Food and Biological Engineering, Jiangsu University, Zhenjiang 212013, China.

[†] Footnotes relating to the title and/or authors should appear here.

Electronic Supplementary Information (ESI) available: [details of any supplementary information available should be included here]. See DOI: 10.1039/x0xx00000x

information simultaneously^{26, 27}, was used to extract the characteristic wavelengths. Then narrowband filters with the corresponding central wavelengths were selected to isolate the effective signal change of the sensor array at the selected wavelengths. Ammonia (NH₃) was taken as example to test the performance of the proposed multi-spectral method. Prediction results based on the multi-spectral information, hyperspectral information and tri-color information were compared.

2. Materials and methods

2.1 Colorimetric sensor array preparation

Colorimetric sensor array is composed of TiO₂ porous film substrate and gas sensitive material. Porphyrins and metalloporphyrins are highly conjugated p-type organic semiconductors, and can induce charge transfer between various oxidizing or reducing gases and their delocalized p-systems. This modifies the optical absorbance as well as electrical conductance significantly, and offers the option of developing both chemiresistive as well as optical gas sensors^{28, 29}. pH indicators are a class of chemical detector sensitive to hydronium ions or hydrogen ions in the Arrhenius model. Normally, an indicator could change its color depending on the pH, and they have been widely used in colorimetric sensors^{30, 31}. Thus, we decided to select sensitive materials from these two classes of chemicals. After several of them were screened,

nine pH indicators and seven Porphyrins/metalloporphyrins (Sigma Chemical, USA) as shown in Fig.S1 (Supplementary information) were selected as the sensitive material. More details about the preparation process of the colorimetric sensor array could be found in previous studies^{21, 32-34} and the Supplementary information.

2.2 Equipment and measurement

2.2.1 Standard NH₃ generation and group assignment

The Permeator Model PD-1B-2 (Gastec Corporation, Japan) was used to generate micro-concentration NH₃ vapor. As shown in Fig.1 (a), gas stream (N₂) containing the vapor of NH₃ was generated from a permeation tube with NH₃ liquor inside. Digital mass-flow controllers were utilized to control N₂ flow speed. More details about the standard NH₃ generation could be found in supplementary information. NH₃ of 7 concentration values (0.5, 1, 2, 3.5, 5, 7.5, 10 ppm), each with 12 replicates, was tested. The humidity was controlled at 50% RH. The 84 (7×12) tested arrays for each concentration were randomly divided into two subsets. The calibration set, consisted of 56 arrays, was used for extraction of the characteristic wavelengths, also for the development of the prediction models based on hyperspectral information and tri-color information. The testing set, consisted of 28 arrays, was used for validation of the developed models. After the multi-spectral sensor array detection system was completed, another 84 arrays were used to test the performance of the multi-spectral method with the same grouping mode.

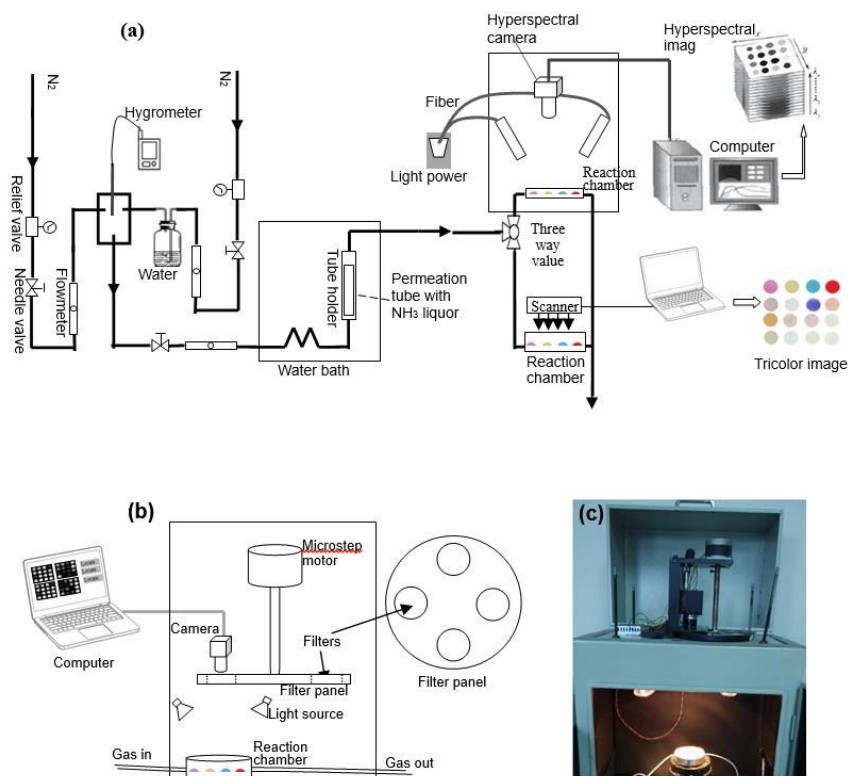


Fig.1 Equipment for standard NH₃ generation, hyperspectral information acquisition, and tri-color information acquisition (a); Schematic diagram (b) and photo (c) of the multi-spectral colorimetric sensor array detection system.

2.2.2 Hyperspectral images acquisition

In order to eliminate the effect of impurities in air, pure N₂ was employed to clean the sensor array in the first 5 min, and then

the array was exposed to NH₃ of needed concentration for 25 min.

The hyperspectral imaging system could collect spectral images in a wavelength range of 430-960 nm with a spectral resolution of 2.73 nm, and more details about the hyperspectral system could refer to our previous reports²⁴.

During image acquisition, the conveyor was driven by the stepping motor with a user-defined speed of 1.58 mm/s, which was adjusted to the camera exposure time to avoid distortion in the spatial resolution of the images. Each array was transported by the conveyor to the field of view (FOV) of the camera, where a raw image was acquired and stored in the computer. The image acquisition process was controlled by SpectralCube software, and finally a hyperspectral image data cube as presented in previous study²⁴ was acquired for each sensor array.

2.2.3 Multi-spectral images acquisition

Fig.1 (b) illustrates the multi-spectral colorimetric sensor array detection system. It is consisted of a filter panel with 4 uniformly distributed narrowband filters (Jingyi high-tech Co.ltd, Beijing, China), a charge-couple device (CCD) camera (XS-1.7-320, Xenics infrared solution, Belgium), three 150 W quartz-halogen DC illuminators (Fiber-Lite PL900-A, Dolan-Jenner Industries Inc., USA), computer, and image processing and analysis software (Matlab R2012a; The Math works, Natick, MA, USA). The whole imaging system was enclosed in a duralumin shield box (350 × 500 × 800 mm) to avoid the interference from external light.

Prior to image acquisition, the multi-spectral imaging system would be opened for preheating for 30 min. During image acquisition, the filter panel was driven by the microstep motor to locate different filters under the camera. Thus, 4 gray-level images at different wavelengths of the sensor array were acquired for each test.

2.2.4 Tri-color images acquisition

Tri-color images were obtained at 1200 dots per inch in RGB color mode using an ordinary flatbed scanner (HP Scanjet G4050). The image before exposed to NH₃ was first acquired on the flatbed scanner; and the array was scanned again after exposed to NH₃ of needed concentration. More details could refer to previous literature²²

2.3 Data analysis

As shown in Fig.2, the data analysis procedure could be roughly divided into two parts, i.e., characteristic wavelengths extraction from the hyperspectral images (Step 1~4) and prediction based on the multi-spectral information (Step 5-8).

(1) Spectra of dye *x* (*x* is the *x*th dye in the array) were extracted from the hyperspectral images of the sensor arrays before and after exposed to NH₃ separately. To avoid factitious nonuniformity, the center of the dye spot (about 400 pixels) was averaged to acquire mean spectrum in the range of 430 to 960 nm². The mean spectrum was pre-processed by moving average (MA) and standard normal variate (SNV) as described in reference^{35, 36}.

(2) The difference spectrum of dye *x* was obtained by differentiating its spectrum before and after exposed to the NH₃ gas. All difference spectra for dye *x* in the calibration set were calculated using the same method.

(3) The correlation coefficient between NH₃ concentrations and the difference values at λ nm (r_{λ}) was calculated according to formula (1).

$$r_{\lambda} = \frac{\sum_{i=1}^n (x_{\lambda,i} - \bar{x}_{\lambda})(y_i - \bar{y})}{\sqrt{\sum_{i=1}^n (x_{\lambda,i} - \bar{x}_{\lambda})^2} \cdot \sqrt{\sum_{i=1}^n (y_i - \bar{y})^2}} \quad (1)$$

Where $x_{\lambda,i}$ represents the value of the difference spectra at λ nm for dye *x* of the *i*th array in the calibration group, y_i is the corresponding NH₃ concentration, \bar{x}_{λ} is the mean value of $x_{\lambda,i}$, \bar{y} is the mean value of y_i , *n* is the total number of the arrays in the calibration set.

The 3 wavelengths with the local optimum *r* were selected as the characteristic wavelengths for dye *x*.

(4) Characteristic wavelengths for all 16 dyes in the sensor arrays were selected according to step (1) ~ step (3).

(5) Four narrowband filters were selected according to the distribution of the characteristic wavelengths for all 16 dyes, and used to develop the multi-spectral colorimetric sensor array detection system as introduced in Section 2.2.

(6) For each test, 4 gray scale images of the sensor array were obtained with changing the selected filters. To quantify the signal change of the dye spot, 4 difference values were obtained from the gray scale images by digitally subtracting the image before exposure to NH₃ from the image after exposure, using a 400-pixel average from the center of each dye spot (thus avoiding subtraction artifacts at the periphery of the spots) as follows.

$$I_{x-\lambda_1-d} = \left| I_{x-\lambda_1-a} - I_{x-\lambda_1-b} \right| \quad (2)$$

$$I_{x-\lambda_2-d} = \left| I_{x-\lambda_2-a} - I_{x-\lambda_2-b} \right| \quad (3)$$

$$I_{x-\lambda_3-d} = \left| I_{x-\lambda_3-a} - I_{x-\lambda_3-b} \right| \quad (4)$$

$$I_{x-\lambda_4-d} = \left| I_{x-\lambda_4-a} - I_{x-\lambda_4-b} \right| \quad (5)$$

Here, *d* represents difference, *a* represents after exposure, *b* represents before exposure, λ_1 , λ_2 , λ_3 , λ_4 are the central wavelengths of the 4 narrowband filters, $I_{x-\lambda_1-d}$, $I_{x-\lambda_2-d}$,

$I_{x-\lambda_3-d}$, $I_{x-\lambda_4-d}$ are the intensity difference of dye *x* with the filtration of the corresponding filters.

(7) Three of the 4 difference values, I_{x-1} , I_{x-2} , I_{x-3} , were used to characterize the signal change of dye *x* according to their optimum wavelength (see Section 3.3). Finally, a 48-dimensional vector (16 dyes×3 intensity differences) was acquired to characterize the signal change of a colorimetric sensor array.

(8) Since too many variables are against the stability of the prediction model, principal component analyses (PCA) was used to decompose the vector into several principal components (PCs), which are uncorrelated and account for the most common spectral variations³⁷. The top 3 PCs contained most of the useful information were used to develop a

multiple regression model with the arrays in the calibration set. Arrays in the testing set was used to test the regression model. In addition, prediction of NH_3 concentration based on hyperspectral information and tri-color information was also performed for comparison purposes. The difference here is the 48-dimensional vector used to characterize the signal of the colorimetric sensor arrays. For prediction based on the

hyperspectral information, the 48-dimensional vector is consisted of the spectrum difference values at the 48 extracted characteristic wavelengths mentioned in step (4). For prediction based on the tri-color information, the 48-dimensional vector is consisted of the R/G/B difference values of the 16 dyes.

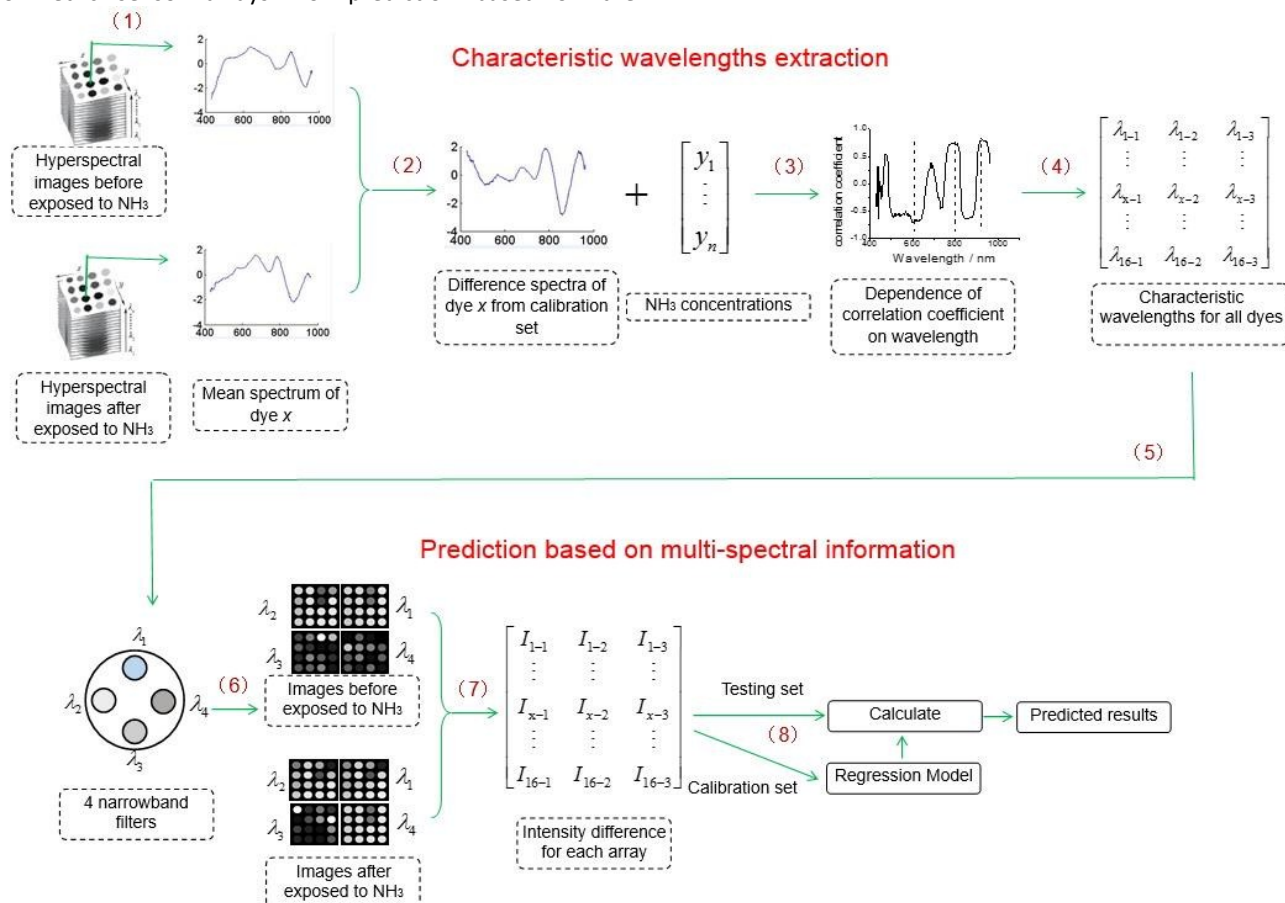


Fig.2 The data analysis flow chart for prediction of NH_3 concentration based on the multi-spectral method.

2.4 Software

All image processing and data analysis procedures described above were executed using programs developed in Matlab R2012a (MathWorks, Natick, MA, USA). Extraction of reflectance spectra from the hyperspectral images was finished using ENVI 4.5 (ITT Visual Information Solutions, Boulder, CO, USA). The software for the multi-spectral colorimetric sensor array detection system was programmed with Visual Basic.net.

3. Results and discussion

3.1 Hyperspectral images investigation

Hyperspectral imaging system acquired abundant spatial information while collecting spectral information. Fig.3 (a) was the combined spectral images at three wavelengths located in the red (670 nm), green (525 nm), and blue (460 nm) regions. Hence, it appeared similar to its natural color. Representative single-band reflectance images of the sensor arrays at 6 selected wavelengths from 430 to 680 nm were shown in Fig.3 to demonstrate general pattern of the hyperspectral images and differences among different spectral regions. When the wavebands increased, the intensity of the dyes showed different trends because of their different colors. As a result, different difference-images which contained abundant information were acquired at different wavelengths.

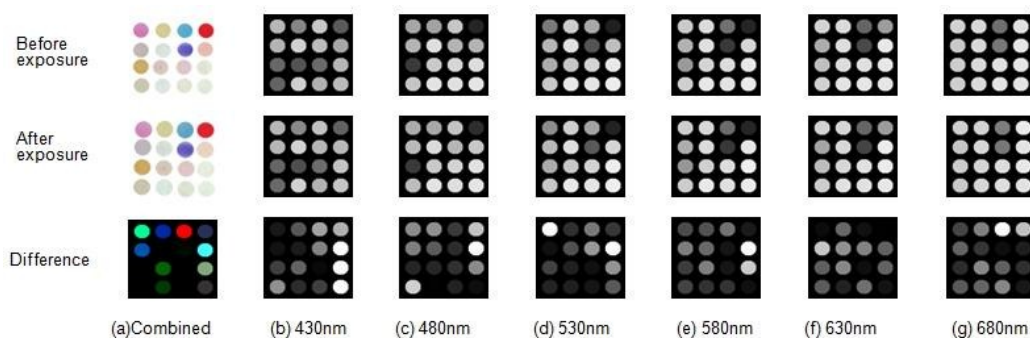


Fig.3 The combined images and images at selected wavelengths from 430 to 680 nm.

3.2 Difference spectra of the dye

Mean spectrum in the range of 430 to 960 nm of each dye were acquired using ENVI 4.5. Then these spectra were pre-processed by MA and SNV sequentially to eliminate variations caused by stochastic noise and baseline drift. The spectrum of a dye before exposed to NH_3 was subtracted from the after one to calculate the difference spectrum as explained in section 2.3.

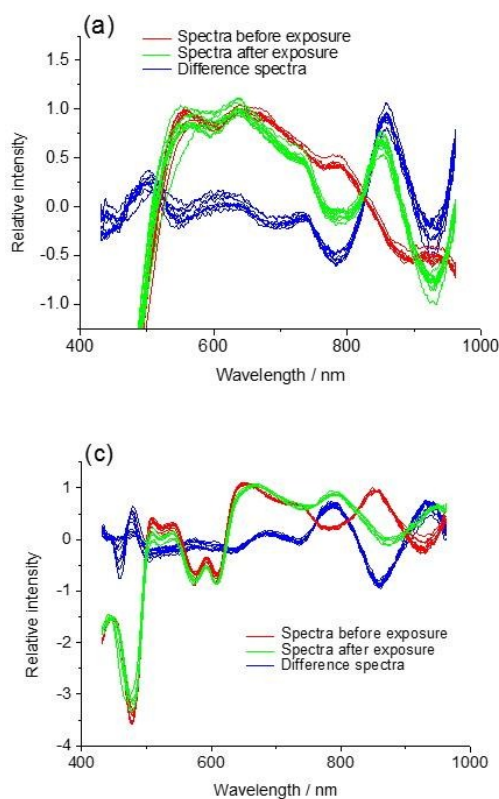
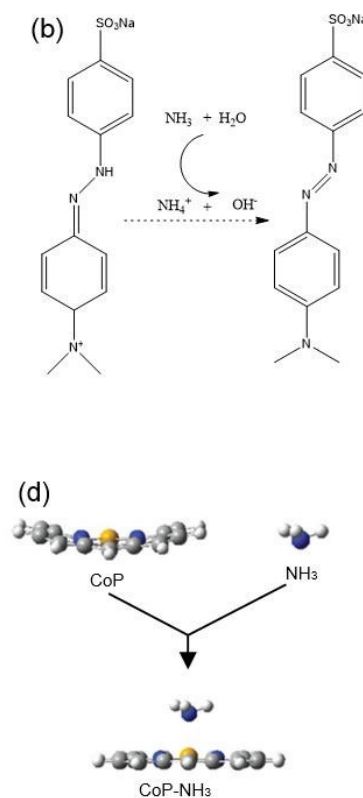


Fig.4 Typical spectra change of pH indicator (illustrate with Methyl orange) (a) and the suggested mechanism for the spectra change (b); Typical spectra change of metalloporphyrin (illustrate with 5,10,15,20-Tetraphenyl-21H,23H-porphine cobalt(II), CoP)(c) and the reaction between CoP and NH_3 (d).

Fig.4 (c) shows the typical spectra change of a metalloporphyrin dye ((5,10,15,20-Tetraphenyl-21H,23H-porphine cobalt(II), CoP) exposed to NH_3 of 7.5 ppm). The spectra showed relatively strong reflection in the bands 510~540 nm and 650~670 nm, which is in consistent with its dark green color. An obvious hypsochromic shift was observed

Fig.4 (a) shows the typical spectra change of a pH indicator (Methyl orange) exposed to NH_3 of 5 ppm. The spectra before exposure showed relatively strong reflection in the bands at 550-650 nm, which agrees well with its antic orange color. An obvious absorption peak at 770 nm was observed after exposed to NH_3 , and the mechanism may be explained as shown in Fig.4 (b)³⁸. NH_3 would ionize to NH_4^+ and OH^- when combined with H_2O , then OH^- attached to Methyl orange, and changed it from acid form to alkali form.



between 680 nm to 960 nm after exposed to NH_3 . The mechanism³⁹ of this response could be explained as Fig.4 (d). An σ -bonding interaction in α -orbitals formed due to the overlap of NH_3 HOMO with the empty orbital of Co, which leads to the electron density transfer from NH_3 molecule to the metal center. In addition, π -bonds formed by back donation from the CoP d_π and p_π orbitals to the π^* -

antibonding orbitals of NH_3 . In β -orbitals, electrons appear to be redistributed around the porphyrin ring. Such electron density transfer finally converts the saddle-like structure into a coplanar one.

Generally, the selected dyes showed good response to NH_3 and different spectrum changes could be observed according to their different molecule structures and reaction mechanisms.

3.3 Extraction of characteristic wavelengths

In order to select the proper narrowband filters to build the multi-spectral colorimetric sensor array detection system, the characteristic wavelengths should be extracted from the hyperspectral images first. The 3 wavelengths with the local optimum r were selected as the characteristic wavelengths for each dye as described in Section 2.3. Fig.5 illustrates the correlation coefficient curve of CoP mentioned in Section 3.2 and its selected 3 characteristic wavelengths (shot dash lines). The optimum characteristic wavelengths for all 16 dyes are listed in Table S1.

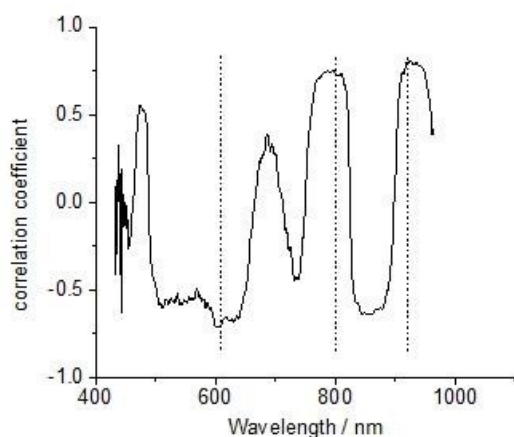


Fig.5 Dependence of the correlation coefficient between NH_3 concentration and the spectrum difference values on wavelength.

3.4 Design of the multi-spectral colorimetric sensor array detection system

As mentioned in step (5) of the data analysis procedure, Fig.6 illustrates the distribution of the optimum characteristic wavelengths for 16 dyes. It was found that the distribution of these wavelengths could be divided into 4 regions roughly. To balance the sensitivity of the involved dyes and ensure the convenience and practicality of the system, mean value of the characteristic wavelengths located in each region (marked with solid lines) was regarded as the center transmission wavelength of one filter. Thus, 4 narrowband filters in total were used to isolate the effective signal change of the sensor arrays at the selected wavelengths. The center transmission wavelength of the 4 filters are 540 ± 2 nm (BP540/10K), 610 ± 2 nm (BP619/10K), 808 ± 2 nm (BP808/10K), 935 ± 5 nm (BP935/30K). Furthermore, the bandwidth of the first 3 filters are 10 ± 2 nm, and the last one is 30 ± 5 nm. The employed filters for each dye to characterize its color change were listed

in Table.1. The structure of the developed multi-spectral colorimetric sensor array detection system was shown in Fig. 1 (b) and (c), and explained in section 2.2.3.

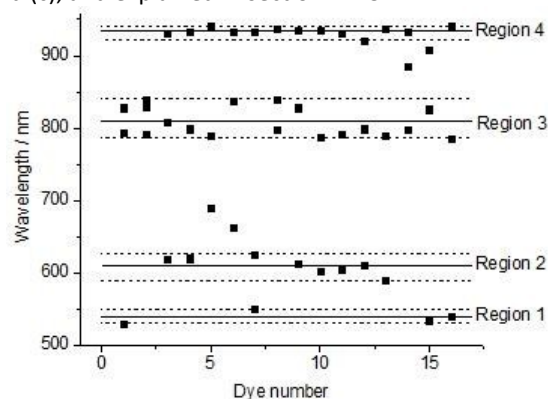


Fig.6 The distribution of the characteristic wavelengths for 16 dyes.

3.5 Performance evaluation of the multi-spectral method

NH_3 was taken as example to test the performance of the proposed multi-spectral method. For each array, 4 gray scale images were obtained with changing the selected filters before and after exposure to NH_3 , separately. A digital image processing technique, as explained in Section 2.3, was applied to quantify the signal change of the sensor array at different wavelengths. Then, 4 difference values were acquired for each dye and 3 of them were used to characterize the signal change according to their optimum wavelength (see Table S1). Finally, a 48-dimensional vector (16 dyes \times 3 intensity differences) was acquired to characterize the signal change of a colorimetric sensor array.

PCA was used to extract information from the acquired vector. Fig.S2 shows the cumulative contributions of the top 10 PCs. It can be seen that the first 3 PCs account for 81.3% accumulation contribution rate, which indicates that the top 3 PCs has the potential to explain 81.3% of the signal change of the sensor arrays. Thus, the top 3 PCs were used to establish the multiple regression model for NH_3 concentration prediction. After tried with several models, a three-variable quadratic equation was selected as the regression model. Results were shown in Fig.7. Several commonly used parameters^{40,41}, i.e., correlation coefficient (R_c for calibration set, R_t for testing set), root mean squared error of cross validation (RMSECV), root mean squared error of prediction (RMSEP) and residual predictive deviation⁴² (RPD_c for calibration set, RPD_t for test set) were used to evaluate the performance of the developed models. The calibration group could be predicted with R_c of 0.976, RMSECV of 0.536 ppm, and RPD_c of 6.167, the testing set with R_t of 0.977, RMSEP of 0.548 ppm and RPD_t of 6.151 respectively. For comparison purposes, prediction of NH_3 concentration based on hyperspectral information and tri-color information was also performed, and the results were shown in Fig.7.

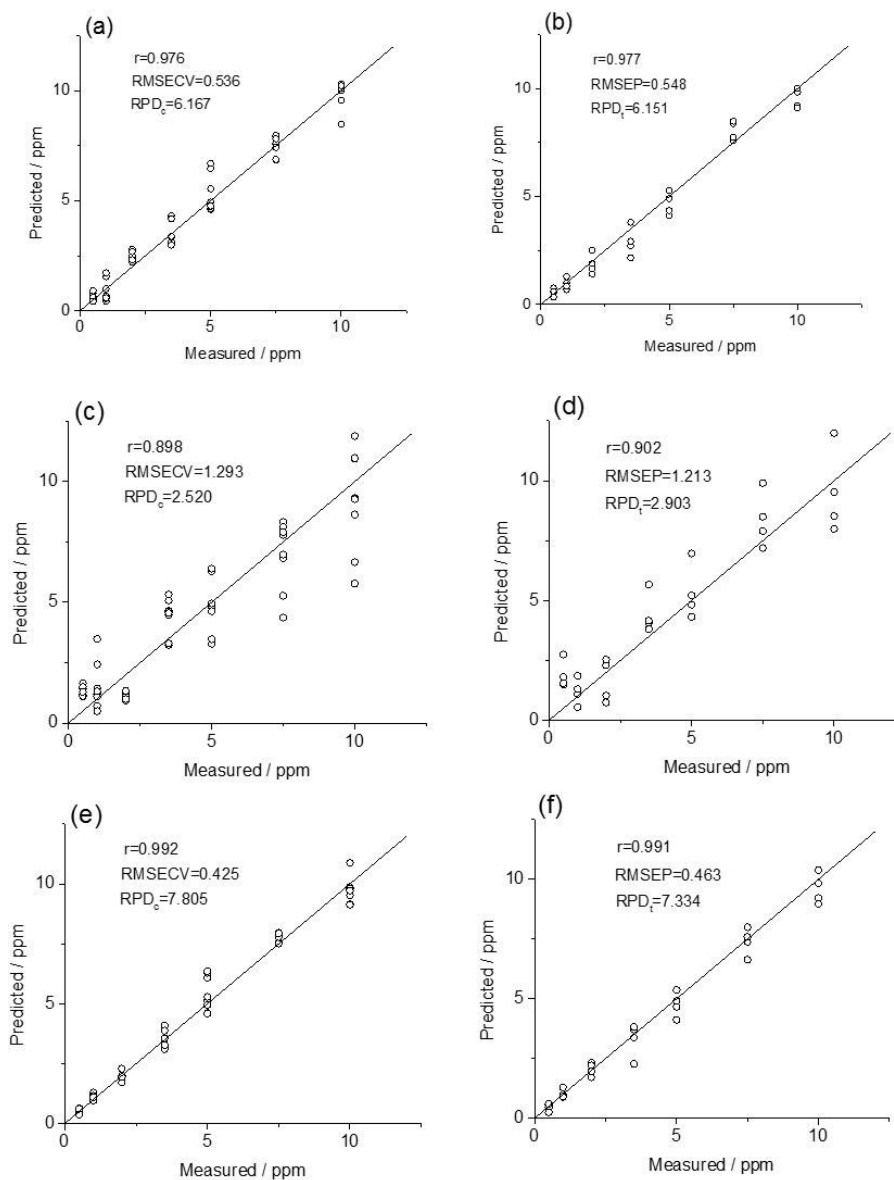


Fig. 7. Prediction results based on the multi-spectral information (a, b), tri-color information (c, d), and hyperspectral information (e, f) for calibration set and testing set, respectively.

Compared with detection based on the traditional tri-color information, R_t based on multi-spectral information increased from 0.902 to 0.976, RMSEP decreased from 1.213 to 0.548, and RPD_t increased from 2.903 to 6.151, which means that the results were improved obviously both in accuracy and stability. It is because the multi-spectral detection system could detect the targeted signal change at the optimum wavelengths more effectively and avoid the interference from other useless wavelength region.

The results also show that measurement based on the multi-spectral information is only slightly less effective than on the hyperspectral information, which is caused by the balance of the sensitivity for the involved dyes. However, it is such a balance make it possible for the multi-spectral method to keep the advantages, such as low-cost, easy operating, greatly reduced data size. Thus, the proposed multi-spectral method is

suitable for the signal characterization of the colorimetric sensor arrays.

4. Conclusions

A multi-spectral method based on the selected narrowband filters was proposed to characterize the signal of the colorimetric sensor arrays. Firstly, the characteristic wavelengths, which are most relevant to the detected substance, were extracted from the hyperspectral information of the colorimetric sensor arrays. Then narrowband filters with the corresponding central wavelengths were selected to isolate the effective signal change of the sensor array at the selected wavelengths. Based on the multi-spectral method, the calibration set could be predicted with R_c of 0.976, RMSECV of 0.536 ppm, and RPD_c of 6.167, the testing set with R_t of 0.977, RMSEP of 0.548 ppm and RPD_t of 6.151 respectively. Results demonstrate that the multi-spectral method shows highly

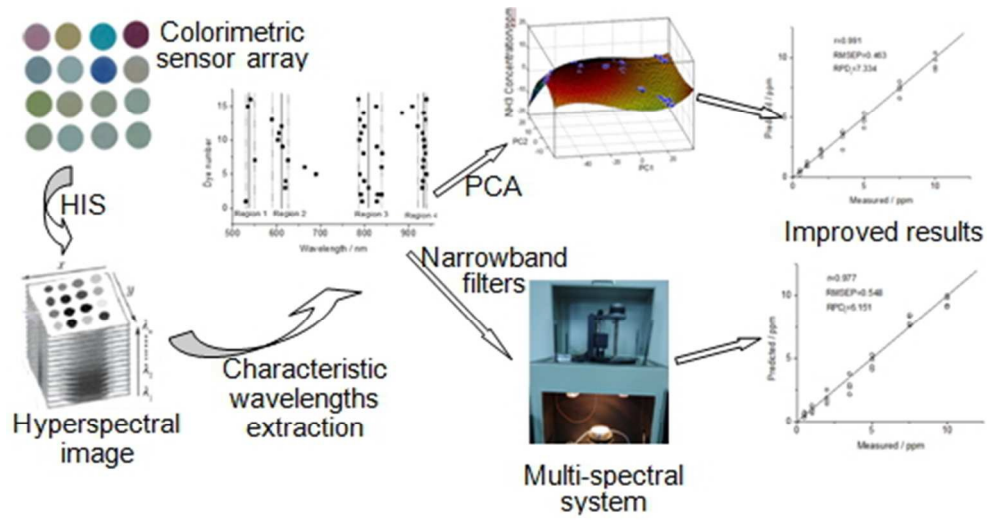
advantageous compared with the tri-color method, both accuracy and stability were improved. Compared with the hyperspectral method, the multi-spectral method possesses the advantages, such as low-cost, easy operating and greatly reduced data size. Thus, the proposed multi-spectral method could be used to characterize the signal of the colorimetric sensor arrays.

Acknowledgements

The authors gratefully acknowledge the financial support provided by the national science and technology support program (2015BAD17B04, 2015BAD19B03), the national natural science foundation of China (Grant No.61301239), the natural science foundation of Jiangsu province (BK20130505), China postdoctoral science foundation (2013M540422, 2014T70483), the Jiangsu province science fund for distinguished young scholars (BK20130010), Science foundation for postdoctoral in Jiangsu province (1301051C), Suzhou science and technology project (SNG201503), Priority Academic program development of Jiangsu higher education institutions (PAPD), Postgraduate innovative program for higher education institutions in Jiangsu province (KYLX15_1094).

References

1. T. Eaidkong, R. Mungkarndee, C. Phollookin, G. Tumcharern, M. Sukwattanasinitt and S. Wacharasindhu, *Journal of Materials Chemistry*, 2012, **22**, 5970-5977.
2. X. Huang, J. Xin and J. Zhao, *Journal of Food Engineering*, 2011, **105**, 632-637.
3. J. H. Bang, S. H. Lim, E. Park and K. S. Suslick, *Langmuir*, 2008, **24**, 13168-13172.
4. B. Guan, J. Zhao, M. Cai, H. Lin, L. Yao and L. Sun, *Analytical Methods*, 2014, **6**, 9383-9391.
5. K. S. Suslick, D. P. Bailey, C. K. Ingison, M. Janzen, M. E. Kosal, W. B. McNamara III, N. A. Rakow, A. Sen, J. J. Weaver, J. B. Wilson, C. Zhang and S. Nakagaki, *Química Nova*, 2007, **30**, 677-681.
6. C. Hou, J. Li, D. Huo, X. Luo, J. Dong, M. Yang and X. Shi, *Sensors and Actuators B-Chemical*, 2012, **161**, 244-250.
7. L. Feng, Y. Zhang, L. Wen, L. Chen, Z. Shen and Y. Guan, *Chemistry-a European Journal*, 2011, **17**, 1101-1104.
8. L. Feng, Y. Zhang, L. Wen, Z. Shen and Y. Guan, *Talanta*, 2011, **84**, 913-917.
9. S. H. Lim, L. Feng, J. W. Kemling, C. J. Musto and K. S. Suslick, *Nat. Chem.*, 2009, **1**, 562-567.
10. L. Feng, C. J. Musto, J. W. Kemling, S. H. Lim and K. S. Suslick, *Chemical Communications*, 2010, **46**, 2037-2039.
11. S. Pumtang, W. Siripornnoppakhun, M. Sukwattanasinitt and A. Ajavakom, *Journal of Colloid and Interface Science*, 2011, **364**, 366-372.
12. M. C. Janzen, J. B. Ponder, D. P. Bailey, C. K. Ingison and K. S. Suslick, *Analytical Chemistry*, 2006, **78**, 3591-3600.
13. P. Zaragoza, A. Fuentes, M. Ruiz-Rico, J.-L. Vivancos, I. Fernández-Segovia, J. V. Ros-Lis, J. M. Barat and R. Martínez-Máñez, *Food Chem.*, 2015, **175**, 315-321.
14. Y. Salinas, J. V. Ros-Lis, J.-L. Vivancos, R. Martínez-Máñez, M. D. Marcos, S. Aucejo, N. Herranz, I. Lorente and E. Garcia, *Food Control*, 2014, **35**, 166-176.
15. L. Feng, C. J. Musto and K. S. Suslick, *Journal of the American Chemical Society*, 2010, **132**, 4046-4047.
16. H. Lin and K. S. Suslick, *Journal of the American Chemical Society*, 2010, **132**, 15519-15521.
17. K. J. Wallace, S. R. Cordero, C. P. Tan, V. M. Lynch and E. V. Anslyn, *Sensors and Actuators B: Chemical*, 2007, **120**, 362-367.
18. M. Y. Jia and L. Feng, *Chin. J. Anal. Chem.*, 2013, **41**, 795-802.
19. L. Feng, H. Li, X. Li, L. Chen, Z. Shen and Y. Guan, *Analytica Chimica Acta*, 2012, **743**, 1-8.
20. P. Anzenbacher, P. Lubal, P. Bucek, M. A. Palacios and M. E. Kozelkova, *Chem. Soc. Rev.*, 2010, **39**, 3954-3979.
21. X. Huang, X. Zou, J. Zhao, J. Shi, X. Zhang, Z. Li and L. Shen, *Meat Science*, 2014, **98**, 203-210.
22. X. W. Huang, X. B. Zou, J. Y. Shi, Y. N. Guo, J. W. Zhao, J. C. Zhang and L. M. Hao, *Food Chem.*, 2014, **145**, 549-554.
23. Z. Xiaobo, S. Jiyong, H. Limin, Z. Jiewen, M. Hanpin, C. Zhenwei, L. Yanxiao and M. Holmes, *Analytica Chimica Acta*, 2011, **706**, 105-112.
24. Z. Xiaobo, Z. Jiewen, M. Holmes, M. Hanpin, S. Jiyong, Y. Xiaopin and L. Yanxiao, *Chemometrics and Intelligent Laboratory Systems*, 2010, **104**, 265-270.
25. Z. Xiaobo, Z. Jiewen, M. J. W. Povey, M. Holmes and M. Hanpin, *Analytica Chimica Acta*, 2010, **667**, 14-32.
26. D. Liu, D. W. Sun and X. A. Zeng, *Food Bioprocess Technol.*, 2014, **7**, 307-323.
27. D. Wu and D. W. Sun, *Innov. Food Sci. Emerg. Technol.*, 2013, **19**, 1-14.
28. M. Biesaga, K. Pyrzyńska and M. Trojanowicz, *Talanta*, 2000, **51**, 209-224.
29. K. Garg, A. Singh, C. Majumder, S. K. Nayak, D. K. Aswal, S. K. Gupta and S. Chattopadhyay, *Org. Electron.*, 2013, **14**, 1189-1196.
30. J. Courbat, D. Briand, J. Damon-Lacoste, J. Wöllenstein and N. F. de Rooij, *Sensors and Actuators B: Chemical*, 2009, **143**, 62-70.
31. A. Y. Mironenko, A. A. Sergeev, S. S. Voznesenskiy, D. V. Marinin and S. Y. Bratskaya, *Carbohydrate Polymers*, 2013, **92**, 769-774.
32. X.-W. Huang, X.-b. Zou, J.-y. Shi, J.-w. Zhao, Y. Li, L. Hao and J. Zhang, *Analytica Chimica Acta*, 2013, **787**, 233-238.
33. H. Chang, C.-M. Hsu, P.-K. Kao, Y.-J. Yang, C.-C. Hsu, I. C. Cheng and J.-Z. Chen, *Journal of Power Sources*, 2014, **251**, 215-221.
34. J.-Y. Liao, B.-X. Lei, D.-B. Kuang and C.-Y. Su, *Energy & Environmental Science*, 2011, **4**, 4079-4085.
35. S. Ji-Yong, Z. Xiao-Bo, Z. Jie-Wen, W. Kai-Liang, C. Zheng-Wei, H. Xiao-Wei, Z. De-Tao and M. Holmes, *Scientia Horticulturae*, 2012, **138**, 190-197.
36. L. Zhang, H. S. Lu, H. W. Yan, Q. Gao, F. J. Wang and H. Y. Song, *Spectrosc. Spectr. Anal.*, 2013, **33**, 3212-3215.
37. R. M. Hathout, *Pharm. Dev. Technol.*, 2014, **19**, 598-604.
38. J. Fan, X. Shen and J. Wang, *Analytica Chimica Acta*, 1998, **364**, 275-280.
39. Z. F. Cao, Q. B. Chen, Y. X. Lu, H. L. Liu and Y. Hu, *Int. J. Quantum Chem.*, 2013, **113**, 1137-1146.
40. L. Huang, J. Zhao, Q. Chen and Y. Zhang, *Food Research International*, 2013, **54**, 821-828.
41. F. Locher, H. Heuwinkel, R. Gutser and U. Schmidhalter, *Agron. J.*, 2005, **97**, 18-25.
42. J. Vongsvivut, M. R. Miller, D. McNaughton, P. Heraud and C. J. Barrow, *Food Bioprocess Technol.*, 2014, **7**, 2410-2422.



46x24mm (300 x 300 DPI)

1
2
3
4
5
6
7
8
9
10
11
12
13
14
15
16
17
18
19
20
21
22
23
24
25
26
27
28
29
30
31
32
33
34
35
36
37
38
39
40
41
42
43
44
45
46
47
48
49
50
51
52
53
54
55
56
57
58
59
60